Simplified receivers for generic binary single side band CPM using PAM decomposition

Karim Kassan, Haïfa Farès, D. Christian Glattli, Yves Louët

▶ **To cite this version:**

Karim Kassan, Haïfa Farès, D. Christian Glattli, Yves Louët. Simplified receivers for generic binary single side band CPM using PAM decomposition. IEEE Access, 2021, 9, pp.115962-115971. 10.1109/ACCESS.2021.3105749 . hal-03367482

HAL Id: hal-03367482
https://hal.science/hal-03367482

Submitted on 6 Oct 2021

HAL is a multi-disciplinary open access archive for the deposit and dissemination of scientific research documents, whether they are published or not. The documents may come from teaching and research institutions in France or abroad, or from public or private research centers.

L'archive ouverte pluridisciplinaire **HAL**, est destinée au dépôt et à la diffusion de documents scientifiques de niveau recherche, publiés ou non, émanant des établissements d'enseignement et de recherche français ou étrangers, des laboratoires publics ou privés.

Distributed under a Creative Commons Attribution 4.0 International License

IEEE Access
Multidisciplinary | Rapid Review | Open Access Journal

Received July 12, 2021, accepted August 12, 2021, date of publication August 18, 2021, date of current version August 26, 2021.

Digital Object Identifier 10.1109/ACCESS.2021.3105749

Simplified Receivers for Generic Binary Single Side Band CPM Using PAM Decomposition

KARIM KASSAN[1], HAÏFA FARÈS[1], D. CHRISTIAN GLATTLI[2], AND YVES LOUËT[1]
[1]IETR-UMR CNRS 6164, CentraleSupélec Rennes Campus, 35576 Cesson-Sevigne, France
[2]SPEC, CEA, CNRS, Université Paris-Saclay, CEA Saclay, Gif sur Yvette, 91191 Paris, France

Corresponding author: Karim Kassan (karimnkassan@gmail.com)

ABSTRACT This paper investigated the pulse amplitude modulation (PAM) decomposition of a class of continuous phase modulation (CPM) signal, which has the property to be a single-side band. We used the PAM decomposition as a convenient solution to provide a large reduced complexity trellis detection to approach the theoretical optimal performance. Moreover, we developed an algorithm to obtain the necessary PAM pulses to approach the optimal performance bound using suboptimal receivers. The algorithm is generic; it can provide the results for any parameter combinations. The proposed demodulation system exhibits excellent performance with minimal complexity with respect to the maximum likelihood sequence detection (MLSD) optimal receiver.

INDEX TERMS Continuous phase modulation (CPM), pulse amplitude modulation (PAM), Laurent decomposition, reduced-complexity receiver, union bound, single side-band (SSB).

I. INTRODUCTION

Continuous phase modulation (CPM) [1] schemes are good candidates for long-distance wireless communication due to their high energy efficiency arising from their constant signal envelopes. For this attractive property, the CPM schemes have been widely used in digital communication systems, e.g., in satellite and deep-space communications, optical fiber, telemetry, etc. In the present paper, we consider a CPM scheme having the original feature of directly generating a single side-band (SSB) spectrum providing a very compact frequency occupation [2]. By *directly*, we mean that SSB property results from the original modulation, not from post-filtering [3]. The new CPM is hereafter called Single Side-Band Frequency Shift Keying (SSB-FSK), which uses a generic phase derivative pulse with a *Lorentzian* shape and a 2π phase increment. The original idea behind the *Lorentzian* pulse and the SSB property was first investigated in quantum physics [4] and [5] with the demonstration of a new quasi-particle called ''Leviton''.

Digital transmissions based on CPM constitute the first immediate applications of *classical levitonics* [6]. In [3], we gave the principle of the modulation and its mathematical justification. In [7], we presented a complete study of the SSB-FSK performance regarding error probability, spectral efficiency, SSB property, and complexity. We investigated the error probability based on the derivation of the minimum squared Euclidean distance. We explored the spectrum of the SSB-FSK by quantifying its signal power bandwidth occupancy using a numerical method. We estimated the complexity from the number of states required by the Viterbi algorithm (VA) to implement the MLSD optimal receiver. Finally, we used these metrics in two different optimization methods to illustrate the full potential of this waveform. Based on this work, we learned that the SSB-FSK has the advantage of being highly tunable and can go beyond what has been achieved with well-known CPM schemes (e.g., RC and GMSK). This work allowed us to determine some interesting configurations, some with acceptable receiver complexity and others requiring more work to design sub-optimal receivers to reduce their high complexity. Therefore, this paper aims to reduce the receiver complexity of the SSB-FSK signals using a suboptimal receiver without affecting the performance. The SSB-FSK signals studied in this work is retrieved from the results obtained in [7] for the specific binary case (modulation level $M = 2$).

A variety of methods have been suggested to decrease the receiver complexity [1], [8]. In this paper, we are particularly interested in using the pulse amplitude modulation (PAM) decomposition of CPM signals.

The associate editor coordinating the review of this manuscript and approving it for publication was Yuan Gao.

This work is licensed under a Creative Commons Attribution 4.0 License. For more information, see https://creativecommons.org/licenses/by/4.0/

A. RELATED WORKS ON CPM PAM DECOMPOSITION

The first connection between linear modulations and CPM was addressed by Laurent [9]. Laurent showed that any binary non-integer single-h CPM could be presented by a superposition of PAM pulses. He also showed that using a reduced number of PAM pulses or even only keeping the main pulse can often approximate very well the CPM signal. Mengali and Morelli followed [10] by extending the PAM decomposition of CPM to M-ary signaling. Then, Huang and Li provided the PAM decomposition for the particular case of CPM schemes with integer modulation index [11]. Soon after, Perrins and Rice [12], and Wylie-Green [13] proposed a generalization of this decomposition to include multi-h CPM schemes. Moreover, Perrins and Rice also developed a PAM decomposition for ternary CPM [14], which was revisited and simplified by Othman *et al.* [15].

Following Laurent's PAM decomposition, Kaleh [16] derived a suboptimal MLSD receiver in AWGN using the PAM decomposition. He also showed that with a considerable decrease in the number of matched filters, the suboptimal PAM-based could reach the optimal MLSD receiver. Moreover, Kaleh provided a boundary for the performance of the suboptimal PAM-based receiver. However, Perrins and Rice [17] showed a lack of accuracy in Kaleh bound. Therefore, they derived an exact performance bound for the suboptimal PAM-based receiver in AWGN channel based on the pairwise error probability. This performance bound has been used to design reduced complexity PAM-based receivers for some CPM schemes [18].

B. MAIN CONTRIBUTIONS

In this paper, a reduced-complexity receiver based on the PAM decomposition is designed and analyzed for binary non-antipodal SSB-FSK. The three key contributions of this paper are:

1) The derivation of a PAM representation for binary non-antipodal SSB-FSK, based on Laurent [9] and Huang and Li [11] PAM decomposition. This representation is not restricted to a specific waveform but could be used for any binary non-antipodal CPM scheme.
2) The design of a simplified receiver for binary SSB-FSK based on Kaleh's [16] suboptimal receiver.
3) The proposal of an algorithm computing the number of PAM pulses required by Kaleh's [16] suboptimal receiver to attain a specific performance bound. This algorithm is based on the performance bound derived by Perrins and Rice [17] and the PAM mean-square approximation [10].

The rest of the paper is organized as follows: we introduced the signal model in Section II. We presented the equivalent PAM representation of SSB-FSK signals for integer and non-integer modulation indices in Section III. Then, in Section IV, we described the MLSD optimal receiver alongside a low-complexity receiver. In Section V, we developed a simple algorithm to decide on the number of PAM pulses required to attain a specific performance bound. The algorithm is generic; it can provide the results for any parameter combinations. In Section VI, we applied the PAM decomposition alongside the algorithm developed on the binary SSB-FSK results retrieved from [7]. In Section VII, we showed that the simplified PAM-based receiver could reach a similar bit error rate (BER) performance compared to the optimal receiver with a considerable decrease in complexity. Finally, conclusions are drawn in Section VIII.

TABLE 1. Table of symbols.

Symbol	Indication
$h, \tilde{h}$	CPM modulation index, SSB-FSK CPM modulation index
L	Pulse length
M	Modulation level
w	Pulse width
α	Transmitted symbol
$E_\mathrm{s}, T_\mathrm{s}$	Energy per transmitted symbol, Duration of the transmitted symbol
μ	2π phase increment correcting factor
$d^2_{\min}, d^2_\mathrm{B}$	Minimum squared Euclidean distance, Minimum squared Euclidean distance upper bound
γ	Difference data sequence
N_s	Number of states needed to implement the MLSD receiver
v_k	PAM pulse
ρ_k	PAM pseudo symbol
ℓ_k	PAM pulse duration
p_k	Optimum MSE PAM pulse
N'_s	Number of states needed to implement the Kaleh PAM receiver
$\mathcal{N}$	Number of PAM main pulses
d'	Modified minimum distance

II. SSB-FSK SIGNAL MODEL

The complex envelope of the SSB-FSK signal is defined as

$$s(t,\alpha) = \sqrt{\frac{E_s}{T_\mathrm{s}}} e^{j\phi(t,\alpha)} \tag{1}$$

$$\phi(t,\alpha) = 2\pi\tilde{h} \sum_{i=-\infty}^{+\infty} \alpha_i \phi_0(t - iT_\mathrm{s}) \tag{2}$$

where E_s is the signal energy per symbol, T_s is the symbol interval, $\tilde{h} = 2h$, where h is the modulation index used to ensure a 2π phase increment, and $\alpha = \{\alpha_i\}$ denotes the information binary sequence. The information symbols α_i are assumed to be independent and identically distributed. It is important to note that no antipodal coding is performed in order to preserve the SSB property, i.e. $\alpha_i \in \{0, 1\}$. Furthermore, $\phi_0(t)$ is a Levitonic phase-shift function [3] and

is given by:

$$\phi_0(t) = \begin{cases} 0 & t < 0 \\ \dfrac{1}{4\pi}\displaystyle\int_{-\infty}^{t} g(\tau)d\tau & 0 \le t < LT_s \\ \dfrac{1}{2} & t \ge LT_s \end{cases} \quad (3)$$

where $g(t)$ is a truncated Lorentzian pulse of duration $LT_s > 1$ (partial-response) symbol durations, defined as

$$g(t) = \frac{d\phi_0(t)}{dt} = \mu\frac{2w^2}{t^2+w^2}, \quad t \in [-LT_s/2, LT_s/2]. \quad (4)$$

The parameter w is the pulse width, and μ is a correcting factor introduced to keep a 2π phase increment after frequency pulse truncation. The correcting factor μ is defined as the ratio between the total phase increment without any truncation and the one obtained after Lorentzian truncation:

$$\mu = \frac{2\pi}{\int_{-LT_s/2}^{LT_s/2}\frac{2w^2}{t^2+w^2}dt} = \frac{\pi}{2\arctan\left(\frac{LT_s}{2w}\right)}. \quad (5)$$

In other words, the derivative of the total phase $\phi(t,\alpha)$ is then a sum of overlapping Lorentzians $\frac{2\mu w^2}{(t-kT_s)^2+w^2}$, centered on kT_s weighted by the symbols α_i and truncated to the length LT_s. For the non-truncated Lorentzian pulse ($L = \infty$), $\mu = 1$ (no correction is required).

III. PAM REPRESENTATION OF SSB-FSK SIGNAL

Despite its originality coming essentially from the Lorentzian pulse, the SSB-FSK signal is nothing else than a CPM signal without any antipodal coding at the symbol level. Therefore, we proposed to apply the same approach given in [9], [11] for the PAM decomposition of CPM signals with integer/non-integer modulation indices. To do so, we had to rewrite the SSB-FSK signal in a way that we could retrieve the same initial assumptions considered in the derivations presented in [9] and [11]. Hence, the signal $s(t,\alpha)$ given in (1) is strictly equivalent to

$$\begin{aligned} s(t,\alpha) &= e^{j2\pi\tilde{h}\sum_{i=-\infty}^{+\infty}\alpha_i\phi_0(t-iT_s)} \\ &= \underbrace{e^{j2\pi h\sum_i\tilde{\alpha}_i\phi_0(t-iT_s)}}_{s_1(t,\tilde{\alpha})}\underbrace{e^{j2\pi h\sum_i\phi_0(t-iT_s)}}_{s_2(t)} \end{aligned} \quad (6)$$

where $\tilde{\alpha}_i = 2\alpha_i - 1 \in \{-1, 1\}$.

According to (6), the baseband SSB-FSK signal $s(t,\alpha)$ could be viewed as a product of two independent signals: $s_1(t,\tilde{\alpha})$, depending on the antipodal coded information symbols $\tilde{\alpha}$, and $s_2(t)$ a *deterministic* signal that does not carry any information.

A. PAM DECOMPOSITION OF SSB-FSK WITH NON-INTEGER MODULATION INDEX

For non-integer modulation indices, we followed the derivations given by Laurent in [9], where $s_1(t,\tilde{\alpha})$ can be reformulated as

$$s_1(t,\tilde{\alpha}) = \sum_{k=0}^{Q-1}\sum_n b_{k,n}c_k(t-nT_s) \quad (7)$$

where $Q = 2^{L-1}$ is the number of pulses required for an exact representation of the signal. The PAM pulse $c_k(t)$ is defined as:

$$c_k(t) = \prod_{i=0}^{L-1} u(t+iT_s+\beta_{k,i}LT_s), \quad 0 \le t \le D_kT_s. \quad (8)$$

The function $u(t)$ is given by

$$u(t) = \begin{cases} \sin(2\pi h\phi_0(t)), & 0 \le t \le LT_s \\ u(2LT_s - t), & LT_s < t \le 2LT_s \\ 0, & \text{otherwise.} \end{cases} \quad (9)$$

Note that the parameters $\beta_{k,i}$ can only take the values 0 or 1, and are obtained from the equality

$$k = \sum_{i=1}^{L-1} 2^{i-1}\beta_{k,i}, \quad 0 \le k \le Q-1. \quad (10)$$

Additionally, D_k is the k-th pulse duration, defined as

$$D_k = \min_i\{L(2-\beta_{k,i}) - i\}, \quad 0 \le i \le L-1. \quad (11)$$

Finally, the mapping between the *pseudo-symbols* and the information data α_i follows the expression

$$b_{k,n} = \exp\left\{jh\pi\left[\sum_{m=-\infty}^{n}\tilde{\alpha}_m - \sum_{i=0}^{L-1}\tilde{\alpha}_{n-i}\beta_{k,i}\right]\right\}. \quad (12)$$

B. PAM DECOMPOSITION OF SSB-FSK WITH INTEGER MODULATION INDEX

For integer modulation indices, we follow the derivations given by Huang and Li [11], stating that the signal $s_1(t,\tilde{\alpha})$ can be represented as

$$s_1(t,\tilde{\alpha}) = \sum_n J^n\left[h_0(t-nT) + \sum_{k=1}^{2^{L-1}}B_{k,n}h_k(t-nT)\right] \quad (13)$$

where $J = \cos(h\pi)$. The PAM pulses $h_0(t)$ and $h_k(t)$ are defined as

$$\begin{aligned} h_0(t) &= \prod_{i=-L+1}^{0}\cos\phi_0(t-iT), \quad 0 \le t \le T \\ h_k(t) &= \prod_{i=1}^{L-1}\cos\phi_0(t-iT)\prod_{i=0}^{L-1}\left[(1-\beta_{k,i})\cos\phi_0(t+iT)\right. \\ &\quad \left.+\beta_{k,i}\sin\phi_0(t+iT)\right], \quad 0 \le t \le L_kT. \end{aligned} \quad (14)$$

The parameters $\beta_{k,i}$ are determined by the equality

$$2k-1 = \sum_{i=0}^{L-1}2^i\beta_{k,i}, \quad 1 \le k \le 2^{L-1}. \quad (15)$$

Additionally, L_k is the k-th pulse duration, defined as

$$L_k = L - \max_{\beta_{k,i}\neq 0} i. \quad (16)$$

Finally, the mapping follows the expression

$$B_{k,n} = \prod_{i=0}^{L-1} \left(1 - \beta_{k,i} + \beta_{k,i} j\tilde{\alpha}_{n-i}\right). \tag{17}$$

We will always refer to these two methods with the same notations, v_k, ρ_k, and ℓ_k, for the PAM pulse, the pseudo symbols, and the pulse duration, respectively.

From what we presented in this section, we could deduce that the PAM decomposition is only applied on the $s_1(t, \tilde{\alpha})$ signal since it contains the complete transmitted information. Thus, the first step on the receiver side is to extract $s_1(t, \tilde{\alpha})$ from $s(t, \alpha)$ by discarding $s_2(t)$, which presents no difficulty since $s_2(t)$ is a deterministic periodic signal with no information. Besides, to assure that we have no degradation in BER performance after discarding $s_2(t)$, in Appendix. A, we showed that $s_1(t, \tilde{\alpha})$ and $s(t, \alpha)$ have the same error probability performance, using the union bound and the minimum squared Euclidean distance ($d^2_{\min}$).

IV. RECEIVER FOR SSB-FSK MODULATION

In this section, we introduced the detection methods used on the received signal. We based our study on the development proposed in [1, ch.7] and [18]. Assuming an additive white Gaussian noise (AWGN) channel, the complex baseband representation of the received signal is

$$r(t) = s(t, \alpha) + n(t), \tag{18}$$

where $n(t)$ is a complex baseband AWGN with zero mean and power spectral density N_0.

A. OPTIMUM MAXIMUM LIKELIHOOD DETECTION

Due to the assumption of AWGN noise, the optimal receiver should be able to find a sequence $\hat{\alpha}$, which maximizes the log likelihood function given by:

$$\Lambda(\hat{\alpha}) = -\int_{-\infty}^{\infty} |r(t) - s(t, \hat{\alpha})|^2 dt. \tag{19}$$

Since $s(t)$ has a constant envelope, minimizing (19) is equivalent to maximizing the correlation function [1]

$$\lambda(\hat{\alpha}) = \mathrm{Re}\left\{\int_{-\infty}^{\infty} r(t) s^*(t, \hat{\alpha}) dt\right\}. \tag{20}$$

Due to the trellis-like structure of the CPM modulation, the computation of the correlation function (20) can be done using the Viterbi Algorithm (VA). To highlight the connection between the VA and the correlation function (20), we need to express the phase trajectories $\phi(t, \alpha)$ as

$$\phi(t, \alpha) = \underbrace{\tilde{h}\pi \sum_{i=-\infty}^{n-L} \alpha_i}_{\theta_n} + \underbrace{2\pi\tilde{h} \sum_{i=n-L+1}^{n} \alpha_i \phi_0(t - iT_s)}_{\theta(t,\alpha_n)}, \quad nT_s \le t \le (n+1)T_s, \tag{21}$$

where the right side $\theta(t, \alpha_n)$ presents the correlative state vectors $(\alpha_{n-1}, \alpha_{n-2}, \ldots, \alpha_{n-L+1})$. The number of all possible correlative state vectors is M^{L-1}. The left side θ_n is the phase state, where the number of phase states could takes only p unique values modulo-2π. The number of phase states p is obtained from the modified modulation index $\tilde{h} = 2m/p$, where $\tilde{h}$ takes only positive rational values. Based on (21), it is now possible to present the SSB-FSK signal in the form of a trellis with a finite number of states, where each branch of the trellis is presented with the starting state (S_n), ending state (E_n), and the $(L+1)$-tuple (σ_n) defined as

$$\begin{aligned} S_n &= (\theta_{n-L}, \alpha_{n-1}, \alpha_{n-2}, \ldots, \alpha_{n-L+1}), \\ \sigma_n &= (\theta_{n-L}, \alpha_n, \alpha_{n-1}, \ldots, \alpha_{n-L+1}), \\ E_n &= (\theta_{n-L+1}, \alpha_n, \alpha_{n-1}, \ldots, \alpha_{n-L+2}). \end{aligned} \tag{22}$$

The total number of states in the trellis is given by

$$N_s = pM^{L-1}. \tag{23}$$

From the arrangement of (21) and the definition of the starting states, ending states, and the $(L+1)$-tuple (S_n, E_n, σ_n) (22), we computed (20) recursively with

$$\lambda_{n+1}(\hat{E}_n) = \lambda_n(\hat{S}_n) + \mathrm{Re}\left\{e^{-j\theta_{n-L}} Z_n(\hat{\alpha}_n, \hat{\theta}_n)\right\}, \tag{24}$$

where $e^{-j\theta_{n-L}}$ is the cumulative phase, and $Z_n(\cdot)$ is the sampled matched filter output, given by:

$$Z_n(\hat{\alpha}_n, \hat{\theta}_n) = \int_{nT_s}^{(n+1)T_s} r(t) e^{-j(\hat{\theta}_n + \theta(t, \hat{\alpha}_n))}. \tag{25}$$

The number of matched filters required for the VA is M^L, obtained from the different possible sequences presented in the $(L+1)$-tuple vector σ_n, and the number of branches pM^L, when considering all possible p phase states.

The performance of the error probability for the SSB-FSK scheme in AWGN noise is quantified by the *Union Bound* [1, ch.3] defined in Appendix. A (38).

A detailed study of the error probability performance for SSB-FSK signals is given in [7].

B. REDUCED-COMPLEXITY RECEIVER FOR SSB-FSK

First, we have to recall that the transmitted signal $s(t, \alpha)$ is composed of two parts: one information-dependent component $s_1(t, \tilde{\alpha})$, and one information-independent component $s_2(t)$. However, so as to use the PAM decomposition, we need to process only $s_1(t, \tilde{\alpha})$. Therefore, after extracting $s_2(t)$ from the received signal $r(t)$, the input of the proposed detector is expressed as

$$r_1(t) = s_1(t, \tilde{\alpha}) + \tilde{n}(t), \tag{26}$$

where $\tilde{n}(t)$ is an equivalent noise resulting from extracting the signal $s_2(t)$, which remains Gaussian. Using the PAM decomposition presented in Section III, we obtained a Viterbi-like receiver based on the PAM decomposition by inserting $s_1(t, \tilde{\alpha})$ (7)/(13) (non-integer/integer modulation index h) into (19) to get the recursion [16]:

$$\lambda_{n+1}(\hat{E}_n) = \lambda_n(\hat{S}_n) + \mathrm{Re}\left\{\sum_{k=0}^{N} \overline{Z}_{k,n} \rho^*_{k,n}\right\}, \tag{27}$$

where

$$\overline{Z}_{k,n} = \int_{nT_s}^{(n+\ell_k)T_s} r_1(t) v_k(t - nT_s) dt. \tag{28}$$

The maximum number of PAM pulses N is given by:

$$N = \begin{cases} Q-1, & \text{(non-integer } h\text{)}, \\ 2^{L-1}, & \text{(integer } h\text{)}. \end{cases} \tag{29}$$

The number of states for the PAM-based detector is [18]

$$N_s' = pM^{L'-1}, \tag{30}$$

where

$$\begin{cases} L' = L + 1 - \ell_{\min}, \\ \ell_{min} = \min\limits_{k} \ell_k, \quad 0 \le k \le N_0. \end{cases} \tag{31}$$

From (27) and (31), we simplified the receiver complexity (number of states and matched filters) by considering a fewer number of pulses [16]. Based on the selection of the number of pulses, the performance and the complexity of the PAM-based receiver may vary. Therefore, it is essential to define thresholds between the number of PAM pulses (complexity) and the performance. In the next section, we will present an algorithm inspired by the methods used in [18] to obtain these thresholds.

V. DECISION ON THE NUMBER OF PAM PULSES

This section discusses how to select the number of PAM pulses for a targeted error probability P_e. In Fig. 1, we presented a flowchart for the associated algorithm used to select the number of PAM pulses. The algorithm depends on two important factors: the PAM pulses obtained from the Mean-Square approximation and the performance bounds of the MLSD and the PAM-based receivers.

A. PAM MEAN-SQUARE APPROXIMATION

Laurent showed in [9] that the signal power is unevenly distributed between the PAM pulses, and for most cases, almost all the power is concentrated in the first few pulses. We will refer to these pulses as the *main pulses*. Laurent obtained a good approximation of the original CPM signals using only the main pulses ($\mathcal{N}$) instead of ($N = Q-1$) pulses. Following Laurent's derivation, Mengali and Morelli [10] showed that a better approximation of the original CPM signals using an optimum PAM pulse $p_k(t)$ instead of $v_k(t)$. This optimum pulse $p_k(t)$ is given by minimizing the mean-square error (MSE) with respect to the original signal. The optimum pulse $p_k(t)$ is given by:

$$p_k(t) = v_k(t) + \sum_{i=\mathcal{N}}^{N-1} \sum_{m} w_{k,i}(m) v_i(t - mT), \quad 0 \le k \le \mathcal{N} - 1, \tag{32}$$

where $w_{k,i}(m)$ are weights whose calculations are detailed in [10].

Furthermore, in [10], it was shown that for a modulation index $h = \frac{1}{2}$, using $p_k(t)$ or $v_k(t)$ has the same performance in approximating the original signal, which means that $v_k(t)$ is already optimal in the MSE sense.

In Table 2, we present the MSE between the original signal and the approximated one using $v_k(t)$ ($\hat{\sigma}$) and $p_k(t)$ ($\tilde{\sigma}$), for three CPM schemes with a different number of main pulses ($\mathcal{N}$). We can observe from the last two columns that we have similar results between ($\hat{\sigma}$) and ($\tilde{\sigma}$). Therefore, we deduced that also for integer modulation index $h = 1$, $p_k(t)$ and $v_k(t)$ have similar performance in approximating the original signal.

TABLE 2. The MSE between the original signal and the approximated one for integer modulation index $h = 1$.

CPM scheme	Number of main pulses $\mathcal{N}$	$\hat{\sigma}$ (dB)	$\tilde{\sigma}$ (dB)
6SSB-FSK ($w = 1.1$)	2	-2.644	-2.643
	4	-11.927	-11.927
3RC	1	-12.083	-12.082
3REC	1	-3	-3

As a consequence, we can find in Fig. 1 a decision box that selects the PAM pulse $p_k(t)$ or $v_k(t)$ based on the modulation index value h.

B. PERFORMANCE BOUND OF THE PAM-BASED RECEIVER

The performance of the PAM-based receiver can be computed using the pairwise error probability union bound given in [17]. The union bound for binary single h schemes is presented in the form

$$P_e \approx \frac{W(\gamma_{\min})}{2^R} \sum_{(i,j)\in\gamma_{min}} Q\left(\sqrt{\frac{E_b}{N_0}} d'(i,j)\right), \tag{33}$$

where γ_{min} (different from zero) is the difference sequence $(\alpha_i - \alpha_j)$ corresponding to the modified minimum distance (d'), and R is the span of observation symbols. The function $W(\gamma_{\min})$ is the Hamming weight of the difference vector γ_{min}. The modified minimum distance d' is given by [19]:

$$d' = \frac{1}{\sqrt{2E_b}} \frac{d_1(\alpha_j, \alpha_i) - d_1(\alpha_i, \alpha_i)}{\sqrt{d_2(\alpha_i, \alpha_j)}} \tag{34}$$

where

$$d_1(\alpha_j, \alpha_i) = \int |\tilde{s}(t; \alpha_j) - s(t; \alpha_i)|^2 dt \tag{35}$$

$$d_1(\alpha_i, \alpha_i) = \int |\tilde{s}(t; \alpha_j) - s(t; \alpha_i)|^2 dt \tag{36}$$

$$d_2(\alpha_i, \alpha_j) = \int |\tilde{s}(t; \alpha_i) - \tilde{s}(t; \alpha_j)|^2 dt \tag{37}$$

with $\tilde{s}(t)$ the approximated signal using $\mathcal{N}$ PAM pulses.

REMARK

The modified Euclidean distance (d') is only an upper bound of the normalized minimum squared Euclidean distance ($d^2_{\min}$) for the PAM-based receiver. Moreover, it is

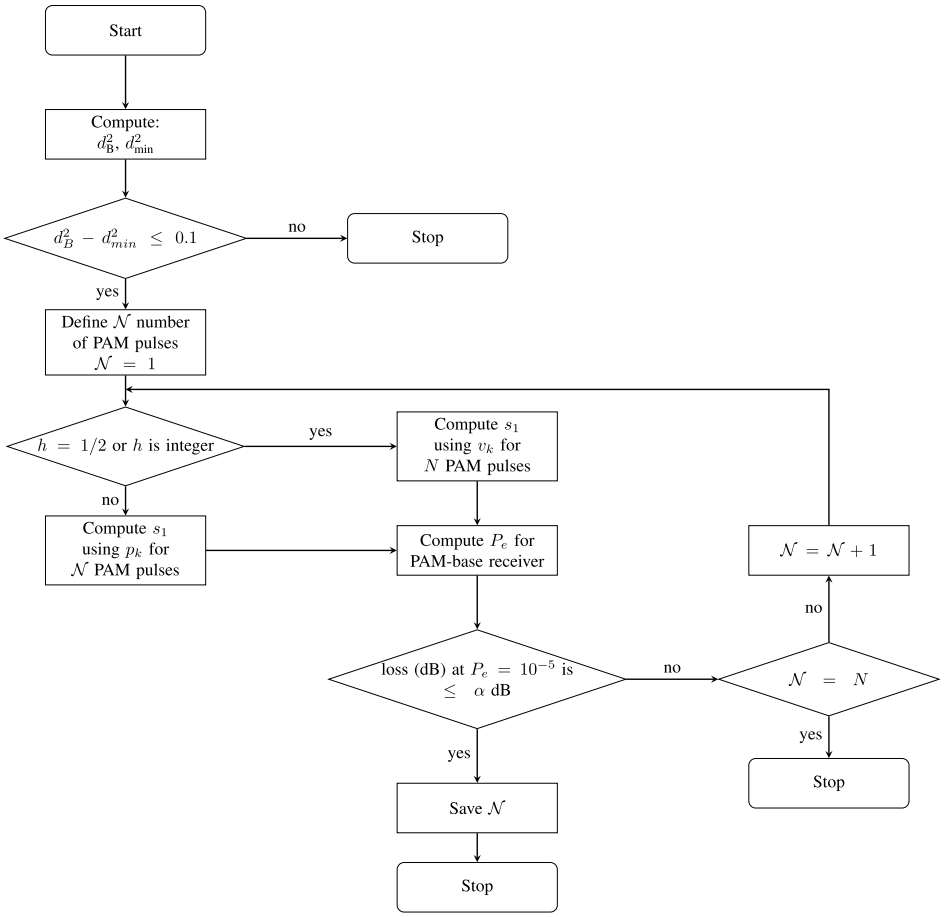

FIGURE 1. Flowchart of the algorithm used to select the number of PAM pulses required for a specific SNR difference α dB between the optimal MLSD receiver performance bound and the PAM-based receiver performance bound for $P_e = 10^{-5}$.

also known from the analysis of the union bound for the optimal receiver that the minimum normalized Euclidean distance d^2_{min} will never reach the upper bound d^2_{B} for several modulation indices h (weak modulation index h [1]). These weak modulation indices h have the same effect on the PAM-based receiver. Due to the high computational efforts on obtaining the exact minimum squared Euclidean distance (d^2_{min}) for PAM-based receiver [1, ch.8], we will always use the upper bound (d') to presents the performance of PAM-based receiver. To ensure that this upper bound (d') is optimal, we first computed the minimum squared Euclidean distance (d^2_{min}) and the upper bound (d^2_{B}) for the optimal receiver. We calculated the difference between the two obtained minimum squared Euclidean distances. If the difference is slight (≤ 0.1), we assumed that the normalized minimum squared Euclidean distance (d^2_{min}) could reach the upper bound (d^2_{B}), which means that the upper bound (d^2_{B}) can present the minimum squared Euclidean distance (d^2_{min}) for the optimal receiver (tight upper bound). Consequently, d' can present the minimum squared Euclidean distance (d^2_{min}) for the PAM-based receiver. Therefore, we can find in Fig. 1 a decision box, which computes the difference between the normalized minimum squared Euclidean distance (d^2_{min}) and the upper bound (d^2_{B}), to tests if it exists an upper bound d' that reaches the error probability P_e.

VI. CASE STUDIES FOR SSB-FSK

We present in this section some case studies for several SSB-FSK schemes, which are showed in Table 3. The parameters selection for these schemes was conducted in [7] using the *Pareto optimum* multi-objective optimization. In Fig. 2, we showed how the performance bound for the PAM-based receiver approaches the optimal MLSD performance bound using the algorithm (Fig. 1) with ($\alpha < 0.5$) for the configuration 6SSB-FSK from Table 3. The plot for $\mathcal{N} = 0$ is not presented, wherefrom (13) $v_0(t)$ ($h_0(t)$) does not carry

TABLE 3. The minimum squared Euclidean distance, the 99.9% bandwidth occupancy, and the complexity (number of states and matched filters) of *L*SSB-FSK studied cases for an optimum MLSD receiver.

Waveform characteristics	d^2_{min}	BW (99.9%)	States (N_s)	Matched filters
6SSB-FSK ($w = 1.1, h = 1$)	3.43	1.226	32	64
2SSB-FSK ($w = 0.6, h = 0.5$)	1.84	1.164	4	8

any information, which means a flat performance bound. Therefore, $v_0(t)$ is not considered in $\mathcal{N}$ as one of the required pulses for the PAM-based receiver. From Fig. 2, we noted that increasing the number of PAM pulses $\mathcal{N}$ sometimes induces a wide leap toward the optimal bound (especially noted between $\mathcal{N} = 3$ and $\mathcal{N} = 4$). Nevertheless, this is not a general trend: after $\mathcal{N} = 4$ increasing $\mathcal{N}$ has a slight increase towards the optimal bound. Then, it is possible to define different thresholds between the required number of PAM pulses (complexity $\mathcal{N}$) and the performance. The performance is computed in terms of SNR required to reach a specific error probability.

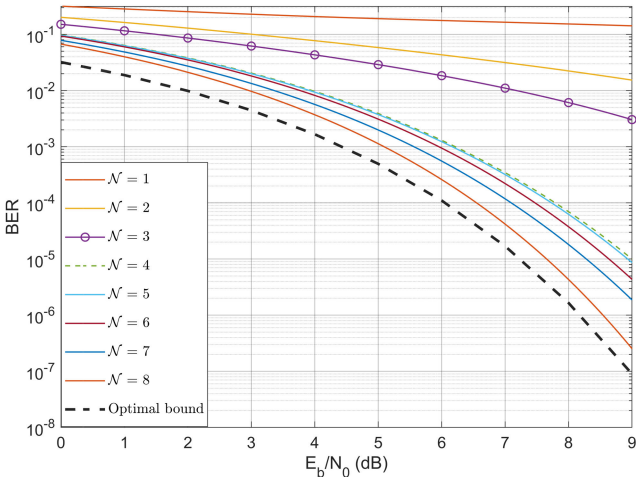

FIGURE 2. Applying the algorithm (Fig. 1) on the first configuration 6SSB-FSK, to obtain the required number of PAM pulses $\mathcal{N}$.

Fig. 3 presents the different PAM pulses for the case study presented in Fig. 2.

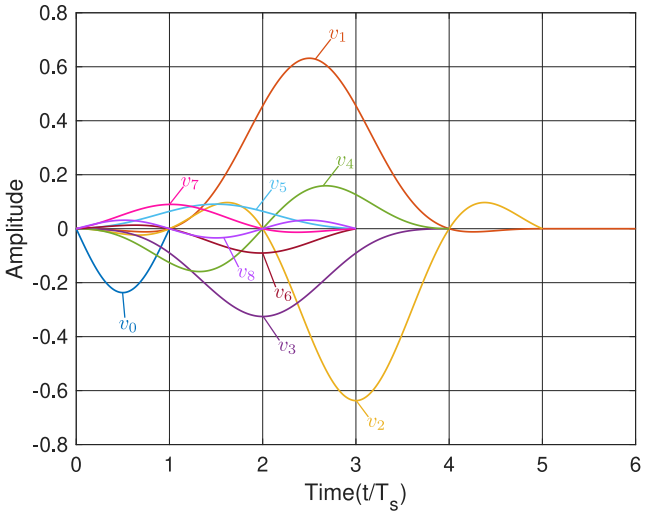

FIGURE 3. The PAM pulses from (0-8) for the configuration 6SSB-FSK using Huang PAM decomposition.

Similarly, in Fig. 4 we showed the performance bound for the PAM-based receiver approaches the optimal MLSD performance bound using the algorithm (Fig. 1) with ($\alpha < 0.5$)

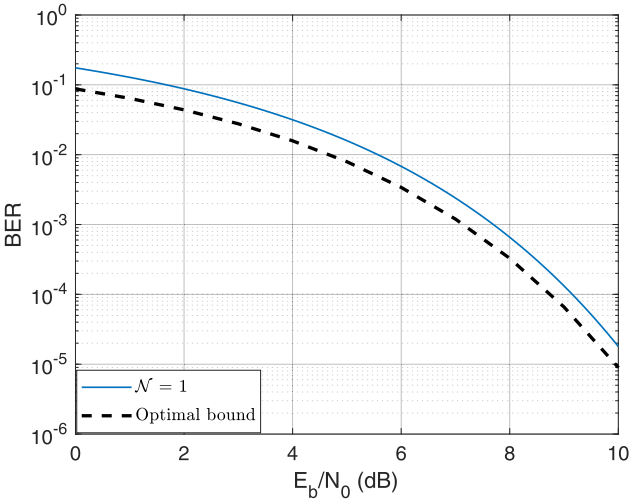

FIGURE 4. Applying the algorithm (Fig. 1) on 2SSB-FSK, the second configuration of Table 3, to obtain the required number of PAM pulses $\mathcal{N}$. bound.

for the configuration 2SSB-FSK from Table 3. We observe that using only one pulse $\mathcal{N} = 1$ leads to the optimal bound. This observation can be explained from Fig. 5, where most of the signal energy is contained in $v_0(t)$.

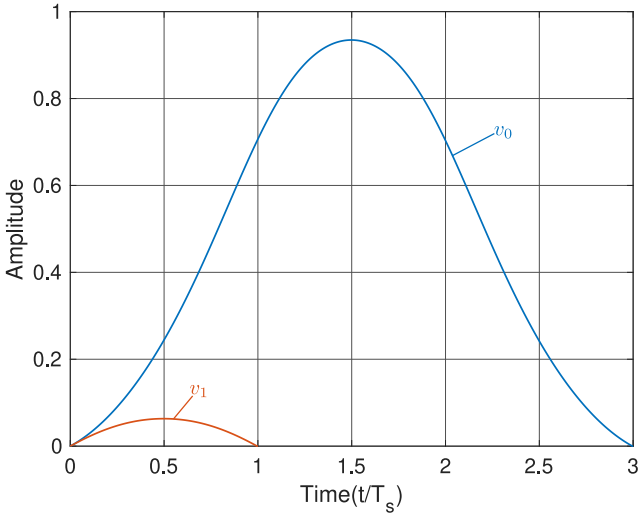

FIGURE 5. The PAM pulses for the configuration 2SSB-FSK using Laurent PAM decomposition.

A. LINEAR DETECTOR

Based on the observation of Fig. 4, we conclude that we only need one pulse to reach the optimal MLSD bound. For this reason, it is interesting to decrease the complexity at the receiver side by applying a linear detector on the received signal instead of the PAM Kaleh receiver.

Following Kaleh's approach in [16], the linear detector is composed of a matched filter $v_0^*(-t)$ followed by a Wiener filter, which plays the role of an equalizer that reduces the effect of intersymbol interference (ISI) from $v_0(t)$ and $v_1(t)$.

In Fig. 6, we presented the coefficients of this filter, which are computed according to [16] for the 2SSB-FSK.

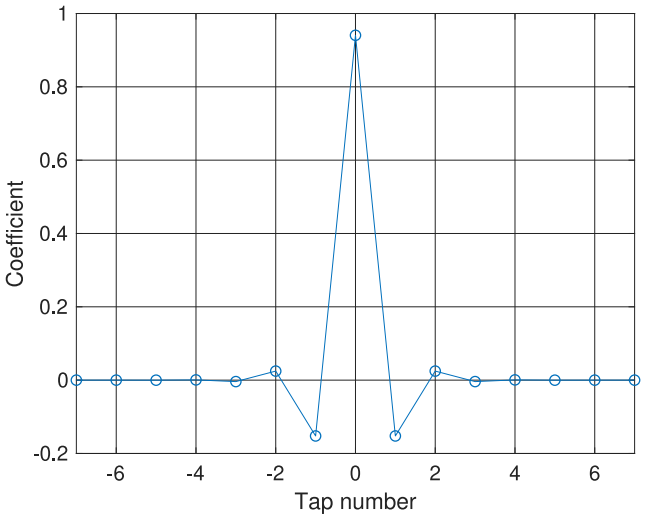

FIGURE 6. Wiener filter coefficients (Eb/N0 = 10 dB) for the configuration 2SSB-FSK.

VII. SIMULATION RESULTS

Fig. 7 shows a BER comparison between the optimal receiver and Kaleh's receiver for 6SSB-FSK. The 8 states receiver is near optimal, as the BER degradation does not exceed 0.1 dB at BER $=10^{-5}$. On the other hand, we obtain a vast decrease in complexity since we went from 32 to 8 for the number of states and 64 to 8 for the number of matched filters. We have also plotted the performance bounds showing a fair reflection of the BER performance, which confirms the results obtained from the algorithm (Fig. 1).

Fig. 8 presents a BER comparison between the optimal MLSD receiver and the linear receiver for the configuration 2SSB-FSK. The linear filter with Wiener filter reaches a BER $= 10^{-5}$ at a SNR slightly lower than the optimal MLSD bound with a loss equal ≈ 0.2 dB. Without the Wiener filter, the degradation increases to ≈ 0.4 dB.

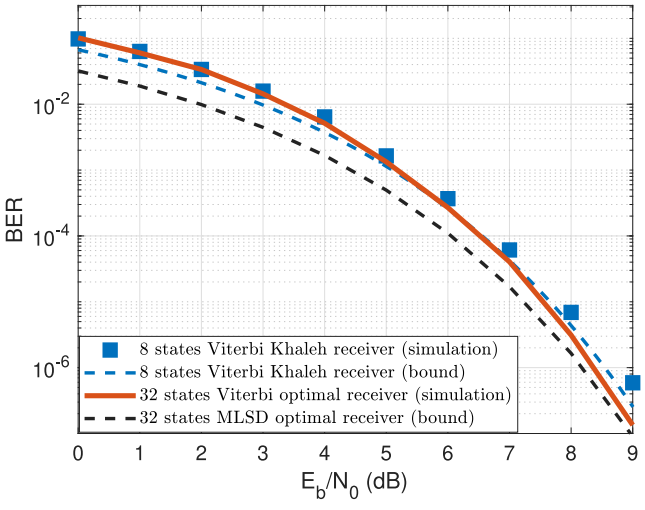

FIGURE 7. BER performance of configuration 6SSB-FSK in AWGN channel.

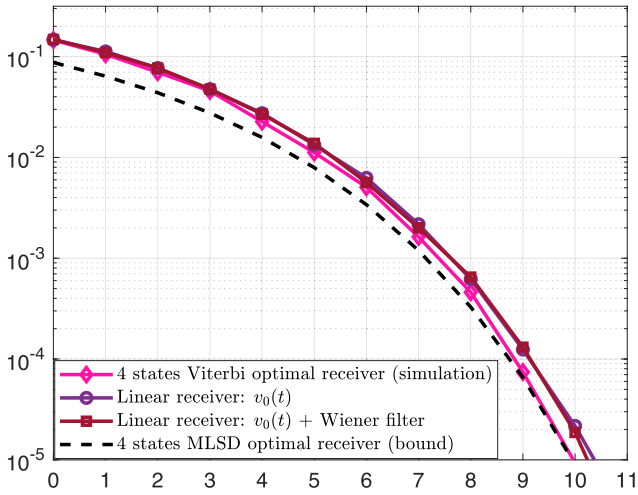

FIGURE 8. BER performance of configuration 2SSB-FSK in AWGN channel.

Table 4 presents the simulation results summary of the BER performance and the receivers complexity for the binary 6SSB-FSK and 2SSB-FSK.

TABLE 4. Reduced-complexity receivers VS. BER performance for binary 6SSB-FSK and 2SSB-FSK.

Receiver type	Waveform characteristics	States	Matched filters	SNR (dB) (BER $=10^{-5}$)
MLSD (Optimal)	6SSB-FSK	32	64	7.5
	2SSB-FSK	4	8	10
Khaleh	6SSB-FSK	8	8	≈ 7.5
Linear	2SSB-FSK	-	1	≈ 10.4
Linear + Wiener	2SSB-FSK	-	1	≈ 10.2

From these results, we can conclude the importance of the PAM decomposition and the algorithm (Fig. 1) in reducing the detection complexity for the SSB-FSK signal.

VIII. CONCLUSION

In this paper, we studied a suboptimal receiver for SSB-FSK CPM schemes using PAM decomposition. First, we obtained the linear PAM decomposition of the non-antipodal integer/non-integer modulation index h SSB-FSK. Using the linear PAM decomposition, we proposed a suboptimal receiver. Due to the PAM decomposition's flexibility, we developed an algorithm with many performance capabilities and with different complexity reductions. One of the most important contributions of this paper is to reduce the complexity at the receiver side using Khaleh and linear receivers based on the PAM decomposition, with an acceptable slight decrease in performance.

APPENDIX A

In this appendix, we show that $s_1(t, \tilde{\alpha})$ and $s(t, \tilde{\alpha})$ have the same error probability performance using the union bound and the minimum squared Euclidean distance. First, let us

define the union bound as presented in [1, Ch. 3, p. 55] for any CPM signal

$$P_e \sim Q\left(\sqrt{d^2_{\min}\frac{E_b}{N_0}}\right), \tag{38}$$

where $d^2_{\min}$ is the minimum squared Euclidean distance. The function $Q(.)$ is the Gaussian error function defined by

$$Q(x) = \int_x^{+\infty} \frac{1}{\sqrt{2\pi}} e^{-v^2/2} dv. \tag{39}$$

To prove that the two signals $s_1(t, \tilde{\alpha})$ and $s(t, \tilde{\alpha})$ have the same error probability, we need to prove that they have the same minimum squared Euclidean distance.

Based on [1, Ch. 3], the general form of the normalized squared Euclidean distance for any CPM signals is given as

$$d^2(\gamma) = \log_2 M\left\{N - \frac{1}{T_s}\int_0^{NT_s} \cos[\phi(t, \gamma_N)]dt\right\}. \tag{40}$$

The variable NT_s is the observation symbol interval, $\boldsymbol{\gamma}$ is the single difference data sequence, where $\boldsymbol{\gamma} = \alpha - \alpha'$, and $\phi(t, \gamma_N)$ is the phase difference trajectories.

Based on (40), it is proved that $s_1(t, \tilde{\alpha})$ and $s(t, \tilde{\alpha})$ have the same $d^2_{\min}$ if they have the same phase difference trajectories $\phi(t, \gamma_N)$. The phase difference trajectories for $s(t, \tilde{\alpha})$ is

$$\phi(t, \gamma) = 2\pi\tilde{h}\sum_i \gamma_i \phi_0(t - iT_s), \tag{41}$$

where the difference sequence γ can take the values $\gamma = \{0, \pm 1\}$ for the binary case ($M = 2$).

Similarly, the phase difference trajectories for $s_1(t, \tilde{\alpha})$ is

$$\tilde{\phi}(t, \tilde{\gamma}) = 2\pi h\sum_i \tilde{\gamma}_i \phi_0(t - iT_s) \tag{42}$$

and the difference sequence $\tilde{\gamma}$ for binary case ($M = 2$) can take the values $\tilde{\gamma} = \{0, \pm 2\}$.

As result, we could easily deduce that $\phi(t, \gamma)$ and $\tilde{\phi}(t, \tilde{\gamma})$ are equal.

As we proved that the two modulations had the same phase difference trajectories, we showed that they had the same minimum normalized Euclidean distance $d^2_{\min}$, and consequently, the same error probability.

REFERENCES

[1] J. B. Anderson, T. Aulin, and C.-E. Sundberg, *Digital Phase Modulation*. New York, NY, USA: Springer, 2013.
[2] H. Farès, D. C. Glattli, Y. Louët, J. Palicot, C. Moy, and P. Roulleau, "From quantum physics to digital communication: Single sideband continuous phase modulation," *Comp. Rendus Physique*, vol. 19, nos. 1–2, pp. 54–63, 2018.
[3] H. Farès, D. C. Glattli, Y. Louët, J. Palicot, P. Roulleau, and C. Moy, "Power spectrum density of single side band CPM using lorenztian frequency pulses," *IEEE Wireless Commun. Lett.*, vol. 6, no. 6, pp. 786–789, Dec. 2017.
[4] J. Dubois, T. Jullien, F. Portier, P. Roche, A. Cavanna, Y. Jin, W. Wegscheider, P. Roulleau, and D. Glattli, "Minimal-excitation states for electron quantum optics using levitons," *Nature*, vol. 502, no. 7473, p. 659, 2013.
[5] T. Jullien, P. Roulleau, B. Roche, A. Cavanna, Y. Jin, and D. Glattli, "Quantum tomography of an electron," *Nature*, vol. 514, no. 7524, p. 603, 2014.
[6] D. Glattli and P. Roulleau, "Method and device for phase modulation of a carrier wave and application to the detection of multi-level phase-encoded digital signals," U.S. Patent 2 016 124 841 A1," Nov. 8, 2016.
[7] K. Kassan, H. Fares, D. Christian Glattli, and Y. Louët, "Performance vs. Spectral properties for single-sideband continuous phase modulation," *IEEE Trans. Commun.*, vol. 69, no. 7, pp. 4402–4416, Jul. 2021.
[8] A. Svensson, C. Sundberg, and T. Aulin, "A class of reduced-complexity viterbi detectors for partial response continuous phase modulation," *IEEE Trans. Commun.*, vol. 32, no. 10, pp. 1079–1087, Oct. 1984.
[9] P. Laurent, "Exact and approximate construction of digital phase modulations by superposition of amplitude modulated pulses (AMP)," *IEEE Trans. Commun.*, vol. 34, no. 2, pp. 150–160, Feb. 1986.
[10] U. Mengali and M. Morelli, "Decomposition of M-ary CPM signals into PAM waveforms," *IEEE Trans. Inf. Theory*, vol. 41, no. 5, pp. 1265–1275, Sep. 1995.
[11] X. Huang and Y. Li, "The PAM decomposition of CPM signals with integer modulation index," *IEEE Trans. Commun.*, vol. 51, no. 4, pp. 543–546, Apr. 2003.
[12] E. Perrins and M. Rice, "PAM decomposition of M-ary multi-H CPM," *IEEE Trans. Commun.*, vol. 53, no. 12, pp. 2065–2075, Dec. 2005.
[13] M. Wylie-green, "A new PAM decomposition for continuous phase modulation," in *Proc. 40th Annu. Conf. Inf. Sci. Syst.*, Mar. 2006, pp. 705–710.
[14] E. Perrins and M. Rice, "PAM representation of ternary CPM," *IEEE Trans. Commun.*, vol. 56, no. 12, pp. 2020–2024, Dec. 2008.
[15] R. Othman, A. Skrzypczak, and Y. Louët, "PAM decomposition of ternary CPM with duobinary encoding," *IEEE Trans. Commun.*, vol. 65, no. 10, pp. 4274–4284, Oct. 2017.
[16] G. K. Kaleh, "Simple coherent receivers for partial response continuous phase modulation," *IEEE J. Sel. Areas Commun.*, vol. 7, no. 9, pp. 1427–1436, Dec. 1989.
[17] E. Perrins and M. Rice, "A new performance bound for PAM-based CPM detectors," *IEEE Trans. Commun.*, vol. 53, no. 10, pp. 1688–1696, Oct. 2005.
[18] E. S. Perrins, "Reduced complexity detection methods for continuous phase modulation," Ph.D. dissertation, Dept. Elect. Comput. Eng., Brigham Young Univ., Provo, UT, USA, Aug. 2005.
[19] M. Wardle and M. Rice, "PAM approach to weak CPM and its application to flight termination receivers," *IEEE Trans. Aerosp. Electron. Syst.*, vol. 44, no. 2, pp. 468–480, Apr. 2008.

KARIM KASSAN was born in Kalamoun, Lebanon, in 1995. He received the B.S. degree in communications and electronics engineering from Beirut Arabic University (BAU), in 2017, and the M.Sc. degree in telecommunications engineering from INSA Rennes, in 2018. He is currently pursuing the Ph.D. degree in signal processing and communication systems with CentraleSupélec, France. His research interests include digital communication theory, wireless communications, synchronization, channel coding, spectrally efficient systems, and complexity reduction receivers.

HAÏFA FARÈS received the bachelor's and M.Sc. degrees in telecommunication engineering from the Higher School of Communications of Tunis (Sup'Com), in 2007 and 2008, respectively, and the Ph.D. degree in digital communications from IMT-Atlantique, France, in 2011. She is currently an Associate Professor at CentraleSupélec of Rennes. She is a member of the Rennes Laboratory (CNRS), Signal Communication Embedded Electronics Research Group, Institute of Electronics and Telecommunications. Her research interests include the area of communication theory, including nonlinear modulations, green communications, iterative decoding algorithms, and non-orthogonal multiple access. She was awarded the best student engineering project, in 2007.

CHRISTIAN GLATTLI born, in 1954. He received the Ph.D. degree from Orsay, in 1986. From 1994 to 2018, he was the Head of the Nanoelectronic Group, CEA Saclay France. He has also founded the Mesoscopic Physics Group, Ecole Normale Supérieure, Paris, in 2000 (led from 2000 to 2012). He is the Research Director at CEA. His main achievements include novel techniques for noise measurements in solids leading to the experimental observation of fractional charge carriers (1999 EuroPhysics PRIZE, 1997 Ancel Prize French Physical Society, and 1998 Silver Medal CNRS), the development of single-electron sources (Science 2007) for flying qubits in electron quantum optics with the discovery of levitons (Nature 2013) enabling electron quantum state tomography (Nature 2014), and the measurement of the Josephson Frequency of e/3 and e/5 anyon charges (SCIENCE 2019). After the discovery of leviton quantum waves, he applied the leviton principle to classical Hertzian waves for digital communications: patent WO2016124841A1.

YVES LOUËT received the Ph.D. degree in digital communications from Rennes University, France, in 2000, and the Habilitation degree (HDR; research) from Rennes University, in 2010. The topic of his Ph.D. thesis regarded peak to average power reduction in OFDM modulation with channel coding. He was a Research Engineer with SIRADEL Company, Rennes, in 2000, and was involved in channel propagation modeling for cell planning. He was also involved in French collaborative research projects, including COMMINDOR, ERASME, and ERMITAGES about channel modeling in many frequency bands, especially, 60 and five GHz for further telecommunication systems. In 2002, he joined Supélec as an Associate Professor. His teaching and research activities were in line with signal processing and digital communications applied to software and cognitive radio systems. He was involved in many collaborative European projects, including FP7E2R, CELTIC B21C, CELTIC SHARING, NoE Newcom, and COST and French projects, including ANR PROFIL, ANR INFOP, WONG5, FUI AMBRUN, APOGEES, TEPN, and WINOCOD. His research contribution is mainly focused on new waveforms design for green cognitive radio and energy efficiency enhancement. In 2010, he became a Full Professor with Supélec and later CentraleSupélec. He is the Head of the Signal Communication Embedded Electronics Research Group, a team from the CNRS Institute of Electronics and Telecommunications, Rennes Laboratory, and the President of the URSI Commission C.